Polarization transition between sunlit and moonlit skies with possible implications for animal orientation and Viking navigation: anomalous celestial twilight polarization at partial moon

András Barta,[1,2,5] Alexandra Farkas,[1,6] Dénes Száz,[1,7] Ádám Egri,[1,2,8] Pál Barta,[2,9] József Kovács,[3,10] Balázs Csák,[3,11] István Jankovics,[3,12] Gyula Szabó,[3,4,13] and Gábor Horváth[1,*]

[1]Environmental Optics Laboratory, Department of Biological Physics, Eötvös University, H-1117 Budapest, Pázmány sétány 1, Hungary

[2]Estrato Research and Development Ltd., H-1121 Budapest, Mártonlak utca 13, Hungary

[3]Gothard Astrophysical Observatory and Multidisciplinary Research Center, Eötvös University, H-9700 Szombathely, Szent Imre herceg utca 112, Hungary

[4]Konkoly Observatory, Hungarian Academy of Sciences, Research Centre for Astronomy and Earth Sciences, H-1121 Budapest, Konkoly Th. M. út 15-17, Hungary

[5]e-mail: bartaandras@gmail.com

[6]e-mail: kfarkasalexandra@gmail.com

[7]e-mail: szaz.denes@gmail.com

[8]e-mail: adam.egri@estrato.hu

[9]e-mail: pbarta@estrato.hu

[10]e-mail: jkovacs@gothard.hu

[11]e-mail: balazs.csak@gmail.com

[12]e-mail: ijankovi@gothard.hu

[13]e-mail: szgy@gothard.hu

*Corresponding author: gh@arago.elte.hu

Received 28 March 2014; accepted 23 June 2014;
posted 1 July 2014 (Doc. ID 208570); published 7 August 2014

Using full-sky imaging polarimetry, we measured the celestial distribution of polarization during sunset and sunrise at partial (78% and 72%) and full (100%) moon in the red (650 nm), green (550 nm), and blue (450 nm) parts of the spectrum. We investigated the temporal change of the patterns of degree p and angle α of linear polarization of sunlit and moonlit skies at dusk and dawn. We describe here the position change of the neutral points of sky polarization, and present video clips about the celestial polarization transition at moonlit twilight. We found that at partial moon and at a medium latitude (47° 15.481′ N) during this transition there is a relatively short (10–20 min) period when (i) the maximum of p of skylight decreases, and (ii) from the celestial α pattern neither the solar–antisolar nor the lunar–antilunar meridian can be unambiguously determined. These meridians can serve as

1559-128X/14/235193-12$15.00/0

reference directions of animal orientation and Viking navigation based on sky polarization. The possible influence of these atmospheric optical phenomena during the polarization transition between sunlit and moonlit skies on the orientation of polarization-sensitive crepuscular/nocturnal animals and the hypothesized navigation of sunstone-aided Viking seafarers is discussed.

OCIS codes: (000.4930) Other topics of general interest; (010.1290) Atmospheric optics; (120.5410) Polarimetry; (110.5405) Polarimetric imaging; (280.1415) Biological sensing and sensors; (290.5855) Scattering, polarization.

http://dx.doi.org/10.1364/AO.53.005193

1. Introduction

The main characteristics of the celestial polarization pattern are well known [1–3]. This knowledge has made remarkable progress over the past few decades due to full-sky (180° field-of-view) imaging polarimetric studies of sky polarization [4–8]. The distribution of skylight polarization has been investigated under clear [9–11], partly cloudy [12,13], overcast [14,15], foggy [15,16], and smoky [17] sky conditions as well as under tree canopies [18]. The polarization characteristics of the sky were also measured under such extreme conditions as total solar eclipses [19–25] and at the edge of ice-sea on the high Arctic [26]. Sky-polarization patterns were also investigated during moonless twilight [27] and at full moon [28]. The polarization pattern of the normal clear sky and the positions of its unpolarized (neutral) points were also measured [11,29,30] and theoretically described [31].

The knowledge accumulated on sky polarization has great biological relevance as well, because many animals, such as birds [32], reptiles [33], amphibians [34], fish [35], insects [36], and crustaceans [37], orient on the basis of the celestial polarization when the sun is invisible. Certain birds have been shown to navigate using polarization cues: they set compasses using skylight polarization at sunset [38,39]. Other animals use sky polarization for short-term orientation [8]. The main reference direction of the orientation of these polarization-sensitive animals is the solar meridian, which is determined from the pattern of angle of skylight polarization when the sun is occluded by clouds. The mirror symmetry axis of this pattern is the solar–antisolar meridian. If the polarization characteristics of the sky are anomalous due to smoke [17] or total solar eclipse [25], for instance, animals orienting by means of the celestial polarization may disorient themselves [38–43].

Although the celestial polarization during twilight has been sporadically studied [27,44,45], and Gál *et al.* [28] compared the polarization of clear moonlit (at full moon) and sunlit skies, the fine details of the transition between the polarization patterns of sunlit and moonlit skies at twilight (sunrise or sunset) have never been investigated. To fill in this gap, using full-sky imaging polarimetry, we measured how the patterns of the degree and angle of skylight polarization change during twilight when the partial (78% and 72%) or full (100%) moon is visible in the sky. The reason for this change is that at sunset the intensity of sunlight scattered in the atmosphere decreases and is gradually overwhelmed by that of the scattered moonlight. Thus, the polarization pattern of the sunlit bright sky is gradually transformed into that of the moonlit dark sky. We show here how the polarization characteristics of the sunlit or moonlit sky differ from those of the moonlit twilight sky. We discuss the possible implications of this transition phenomenon on the orientation of polarization-sensitive crepuscular/nocturnal animals and the hypothesized navigation of sunstone-aided Viking seafarers. We also present here video clips demonstrating this celestial polarization transition during moonlit twilight.

2. Materials and Methods

A. Full-Sky Imaging Polarimetry

Our full-sky imaging polarimetric measurements were performed with a three-camera imaging polarimeter and cloud detector developed by Estrato Ltd. (Budapest) and set up at the roof of a building of the Gothard Astrophysical Observatory and Multidisciplinary Research Center of the Eötvös University in Szombathely, Hungary (47° 15.481′ N, 16° 36.213′ E). The instrument contains three cameras (Imaging Source DFK41BU02, Germany) with fisheye lenses (Fujinon FE185C046HA-1, Japan) and fixed linear polarizers (Edmund Optics, 43-785, USA) in the optical paths. The three polarizers had directions of transmission axis of 100.27°, 45.39°, and 142.28° measured clockwise from the vertical of the camera image sensor. The three cameras took the polarization pictures required for linear polarimetry simultaneously with identical settings.The parallax error was negligible, because the sky was practically at an infinite distance from the polarimeter. Raw red, green, and blue values (measured to be linear as a function of the incident light intensity) of the cameras' Bayer filters were used for image processing. In each camera the 5 mm diameter circular image of the fisheye lens was projected onto the CCD detector (6.3 mm × 4.7 mm). This caused a small crescent of the image's upper or lower part to be out-of-detector (called CCD-void in this work). As two cameras were mounted with the same orientation while the third one was mounted with a 180° rotation along the vertical optical axis, this crescent appears on both lower and upper parts of the evaluated images.

B. Celestial Positions of the Sun and Moon

The azimuth and elevation angles of the sun and moon were determined by the algorithms of Meeus [46], taking the atmospheric refraction into account.

C. Finding the Symmetry Axis of the Celestial Pattern of the Angle of Polarization

The pattern of the angle of polarization α of skylight contains the direction (angle) of polarization in a given sky pixel with respect to the local meridian. This pattern is antisymmetric to the solar–antisolar meridian. To make it symmetric, 90° was subtracted from the α value; then the absolute value was calculated, resulting in the symmetrized α' value for each pixel:

$$\alpha' = |\alpha - 90°|. \tag{1}$$

The direction (angle θ) of the symmetry axis of the symmetrized α' pattern was calculated by means of the image moments [47]: the raw moments of a spectral channel of a given image can be calculated as

$$M_{jk} = \iint f(x,y) \cdot x^j y^k \cdot \mathrm{d}x \cdot \mathrm{d}y, \tag{2}$$

where $f(x,y)$ is the intensity value of the image at coordinates (x,y) in a given spectral range. M_{00} is the image power, and $M_{10}/M_{00} = x_c$ and $M_{01}/M_{00} = y_c$ are the coordinates of the image center. The central moments of the image are defined by

$$\mu_{jk} = \iint f(x,y) \cdot (x - x_c)^j \cdot (y - y_c)^k \cdot \mathrm{d}x \cdot \mathrm{d}y. \tag{3}$$

The angle of the symmetry axis of the symmetrized α' pattern is [47]

$$\theta = \frac{1}{2} \arctan\left(\frac{2\mu_{11}}{\mu_{20} - \mu_{02}}\right). \tag{4}$$

For these calculations the original full-sky images were cropped to half of their width and height to exclude image areas containing trees and antennas.

D. Finding the Position of Neutral Points

In the patterns of the degree of linear polarization p compact sky areas were detected, where $p < p^*$. By choosing the p^* value ($p^* \approx 10\%$) as well as the minimum and maximum size limits (pixel number) of these compact areas appropriately, there were only two such sky regions, the centers of which were considered as the positions of the neutral points of sky polarization. The angular distance of such a center from the zenith and the image vertical gave the zenith angle and the azimuth angle of a neutral point, respectively. Depending on species, the range of the threshold of polarization sensitivity in animals is $5\% < p^* < 25\%$ [8].

E. Simulating Skylight Polarization

To simulate the skylight polarization patterns during the transition between sunlit and moonlit skies, a mix of the polarization patterns of the sunlit and the moonlit sky was calculated. For a given position of the celestial light source (sun or moon) the intensity distribution was calculated on the basis of the single-scattering Rayleigh model [3]. The degree and angle of linear polarization patterns were calculated using the model of Berry *et al.* [31]. For every celestial point the Stokes components (I, Q, U) of skylight were calculated from the intensity I, degree p, and angle α of polarization [48] for a given solar position as well as for a given lunar position. These two patterns of the Stokes components were summed element by element with a given weight w characterizing the contribution of scattered moonlight to sky polarization relative to that of scattered sunlight (for example, $w = 1$ means that scattered moonlight and skylight have an equal contribution to the net polarization of skylight). Finally, from the summed Stokes components the patterns of I, p, and α of the sunlit and moonlit sky were calculated and visualized.

3. Results

Figures 1–4 show the photographs and the patterns of the degree of linear polarization p and angle of polarization α of the clear sky measured by full-sky imaging polarimetry in the blue (450 nm) part of the spectrum after sunset (Figs. 1 and 2) and prior to sunrise (Figs. 3 and 4) on four different days when 78% (Fig. 1), 100% (Figs. 2 and 3), and 72% (Fig. 4) of the moon disc was sunlit. Until scattered sunlight dominated the sky (Fig. 1A), the solar Arago (sAr) and Babinet (sBa) neutral points of skylight polarization occurred in the p patterns (Fig. 1B). When scattered moonlight dominated (Fig. 1G), the lunar Babinet (ℓBa) and Brewster (ℓBr) neutral points appeared (Fig. 1H). In the α patterns these neutral points were positioned where α suddenly had 90° of change along a meridian (Figs. 1C and 1I). The mentioned neutral points occurred along the solar–antisolar (Figs. 1B and 1C) and the lunar–antilunar (Figs. 1H and 1I) meridians when sunlight (Fig. 1A) and moonlight (Fig. 1G) were dominating, respectively. When, however, sunlight and moonlight competed (Fig. 1D), the sN neutral point (closer to the sun) and the ℓN neutral point (closer to the moon) were positioned off both the solar–antisolar and the lunar–antilunar meridians (Figs. 1E and 1F).

In Fig. 2 it can clearly be seen that at full moon the sAr and sBa as well as the ℓAr and ℓBa neutral points were positioned along the solar–antisolar and lunar–antilunar meridians, respectively. In the intermediate situation, when scattered sunlight and moonlight competed (Fig. 2D), the nomenclature of neutral points is dual: the neutral point near the sun can be named as either the solar Babinet or lunar Arago point, while the neutral point near the moon can be called either the lunar Babinet or solar Arago point (Figs. 2E and 2F). Other polarization

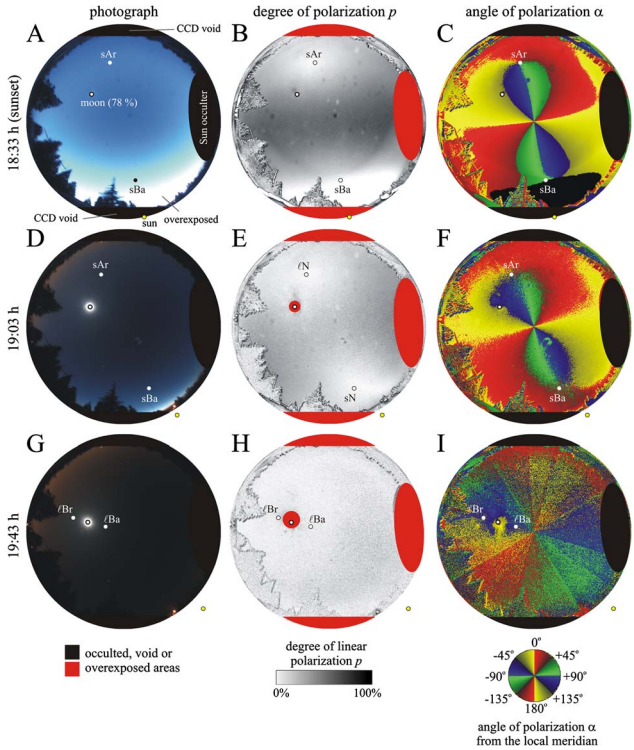

Fig. 1. Photographs and patterns of the degree of linear polarization p and angle of polarization α (clockwise from the local meridian) of the clear sky measured by full-sky imaging polarimetry in the blue (450 nm) part of the spectrum after sunset in Szombathely, Hungary (47° 15.481′ N, 16° 36.213′ E) on 22 March 2013 when 78% of the moon disc was sunlit. (A)–(C) 18:33 h (= local winter time = GMT+1 h, where GMT is Greenwich Mean Time). (D)–(F) 19:03 h. (G)–(I) 19:43 h. The small patches in the pictures and p patterns are due to raindrops on the plexi-dome of the polarimeter. The positions of sun (below the horizon), moon (above the horizon), and neutral points of skylight polarization are shown by dots. sAr, solar Arago neutral point; sN, solar neutral point; ℓN, lunar neutral point; sBa, solar Babinet neutral point; ℓBa, lunar Babinet neutral point; ℓBr, lunar Brewster neutral point.

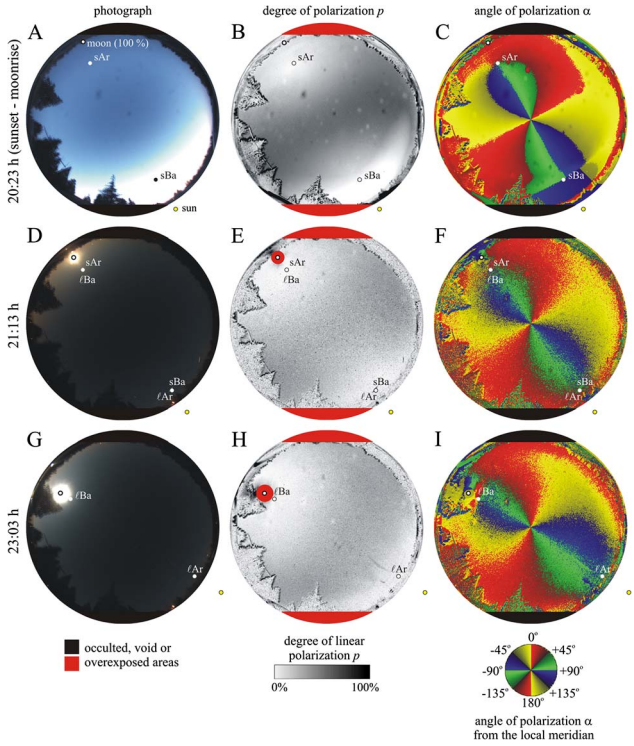

Fig. 2. Same as Fig. 1 after sunset/moonrise on 25 April 2013 when 100% of the moon disc was sunlit (full moon). (A)–(C) 20:23 h (= GMT + 2 h). (D)–(F) 21:13 h. (G)–(I) 23:03 h. sAr: solar Arago neutral point, sBa, solar Babinet neutral point; ℓBa, lunar Babinet neutral point; ℓAr, lunar Arago neutral point.Pattern of α, where black bars show the average local direction of polarization (Media 1) Simulated α pattern with weight $w = 1$, meaning that the contributions of scattered sunlight and moonlight to sky polarization are equal (Media 2). Pattern of $|\alpha - 90°|$, where black and white pixels correspond to directions of polarization perpendicular and parallel to the local meridian, respectively, yellow and blue lines show the solar and lunar meridians, respectively, and the green line shows the axis of mirror symmetry of sky polarization (Media 3). Pattern of $|\alpha - 90°|$, where the red overlay shows sky areas where the degree of linear polarization p is less than 10% (Media 4). All four video clips show the patterns from 19:23 h on 25 April 2013 to 06:03 h on 26 April 2013 during dusk, night, and dawn in the blue spectral range when 100% of the moon disc was sunlit. (Yellow and blue dots show the solar and lunar positions, respectively.)

characteristics of the sky at full moon in Fig. 2 were similar to those in Fig. 1.

According to Fig. 3, prior to sunrise at full (100%) moon the transition of celestial polarization between moonlit and sunlit skies is similar to that between sunlit and moonlit skies at full moon after sunset (Fig. 2); only the temporal order of changes is reversed. Similarly, according to Fig. 4, prior to sunrise at partial (72%) moon the transition of sky polarization between moonlit and sunlit skies is similar to that between sunlit and moonlit skies at partial (78%) moon after sunset (Fig. 1); only the temporal order of changes is reversed.

Figure 5 shows p_{max} of skylight measured in the green (550 nm) averaging the p values in small circular celestial regions at 90° from the sun and moon as a function of time for the four different twilight situations in Figs. 1–4. For Figs. 5B and 5C these two circular sky regions overlap almost completely, because the moon is located practically at the antisolar point. In these cases the average p_{max} was calculated in the union of the two regions.

According to Fig. 5A, prior to sunset p_{max} created by the sun is significantly higher than that created by the moon, but these two p_{max} values gradually decrease and merge after sunset. The same phenomenon occurs during sunrise, but in reverse order (Fig. 5D): before sunrise the p_{max} values created by the sun and the moon are almost the same, and they separate after sunrise in such a way that the sun will create higher p_{max} than the moon.

At full moon p_{max} values created by the sun and the moon are located at the same celestial region. As seen in Fig. 5C, p_{max} gently decreases with time until sunrise, and then increases rapidly after sunrise, reaching a peak at 61%. In Fig. 5B the same can be seen in a reverse order: p_{max} peaks (63%) just before sunset, and then rapidly decreases. In Fig. 5B,

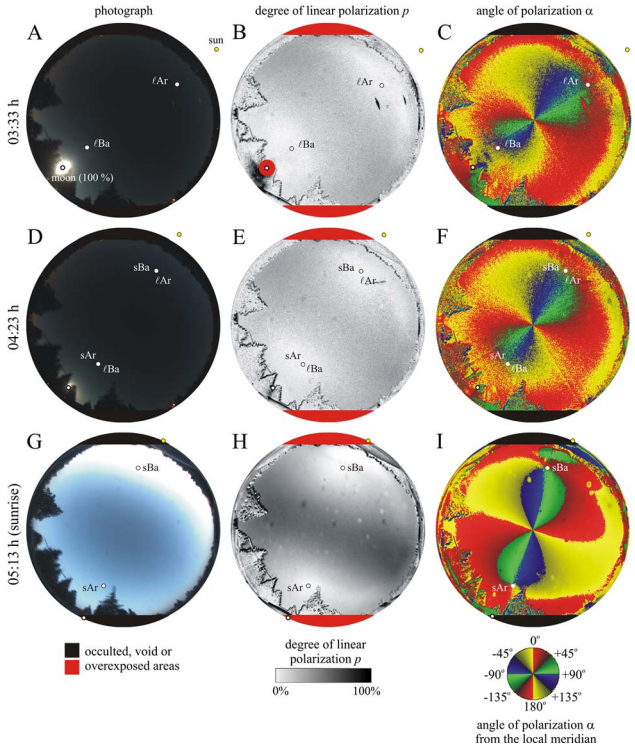

Fig. 3. Same as Fig. 1 prior to sunrise on 26 April 2013 when 100% of the moon disc was sunlit (full moon). (A)–(C) 03:33 h (= GMT + 2 h). (D)–(F) 04:23 h. (G)–(I) 05:13 h. ℓBa, lunar Babinet neutral point; ℓAr, lunar Arago neutral point; sAr, solar Arago neutral point; sBa, solar Babinet neutral point.

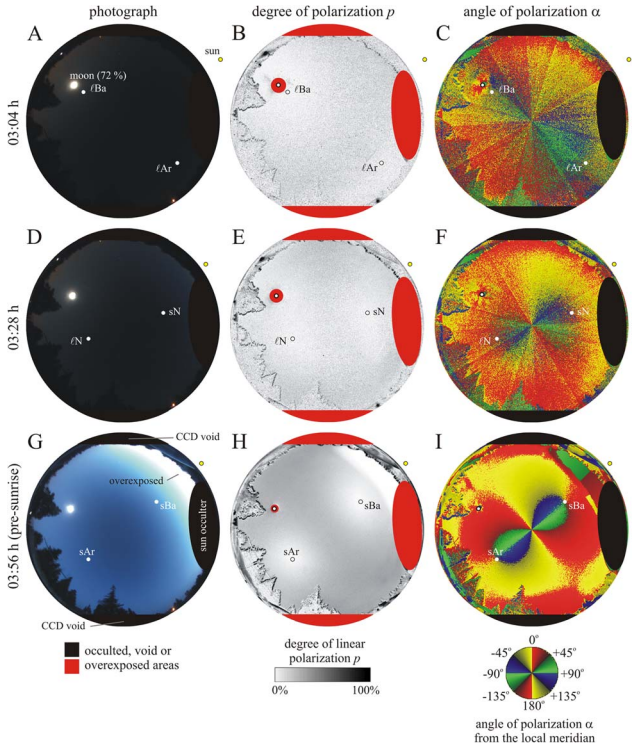

Fig. 4. Same as Fig. 1 prior to sunrise on 28 June 2013 when 72% of the moon disc was sunlit. (A)–(C) 03:04 h (= local summer time = GMT + 2 h). (D)–(F) 03:28 h. (G)–(I) 03:56 h. ℓBa, lunar Babinet neutral point; ℓAr, lunar Arago neutral point; sN, solar neutral point; ℓN, lunar neutral point; sAr, solar Arago neutral point; sBa, solar Babinet neutral point. Pattern of α, where black bars show the average local direction of polarization (Media 5). Pattern of $|\alpha - 90°|$, where black and white pixels correspond to directions of polarization perpendicular and parallel to the local meridian, respectively, yellow and blue lines show the solar and lunar meridians, respectively, and the green line shows the axis of mirror symmetry of sky polarization (Media 6). Pattern of $|\alpha - 90°|$, where the red overlay shows sky areas where the degree of linear polarization p is less than 10% (Media 7). All three video clips show the patterns in the blue spectral range from 02:07 to 06:00 h on 28 June 2013 during dawn when 72% of the moon disc was sunlit. (Yellow and blue dots show the solar and lunar positions, respectively.)

after sunset p_{max} has another, quite small, peak. However, this is an artifact due to a caustic created by the reflection from the plexi-dome of our imaging polarimeter. In Fig. 5B the dashed line represents the expectation. Both at partial and full moon, immediately before sunrise or after sunset, p_{max} has a minimum (Fig. 5).

Figure 6A shows the azimuth angle of the sun, moon, and symmetry axis of sky polarization versus time in the red, green, and blue parts of the spectrum when 72% of the moon disc was sunlit for the situation in Figs. 4 and 5D. In Fig. 6A it can be seen how the symmetry axis, coinciding with the meridian along which the two neutral points (ℓAr and ℓBa, then sN and ℓN, later sAr and sBa) are placed, changes from the lunar meridian to the solar meridian. When scattered moonlight dominated the sky (Figs. 4A–4C), the symmetry axis of celestial polarization coincided with the lunar–antilunar meridian. If scattered sunlight was dominating in the sky (Figs. 4G–4I), the symmetry axis of sky polarization coincided with the solar–antisolar meridian. When scattered moonlight and sunlight competed (Figs. 4D–4F), the symmetry axis of sky polarization was intermediate in such a way that it switched from the lunar–antilunar meridian to the solar–antisolar meridian prior to sunrise (Fig. 6A), and *vice versa*, from the solar–antisolar meridian to the lunar–antilunar meridian after sunset. Prior to this switch, the symmetry axis slightly deviated (delayed/fell behind) from the lunar–antilunar meridian: the azimuth angle of the former was slightly larger than that of the latter for a short transient period (Fig. 6A). This transition of the symmetry axis between the lunar–antilunar and solar–antisolar meridians had a slight dispersion: the transition happened first in the blue, then in the green, and finally in the red spectral range (Fig. 6A).

Figure 6B represents the zenith angle θ_{Ba} of the lunar Babinet neutral point ℓBa as a function of time for the same situation as in Fig. 6A. The neutral point ℓBa first neared the zenith; then reaching its minimal θ_{Ba} it gradually moved away from the zenith in all three spectral ranges. Note that the neutral points are positioned at the tips of the green–blue eight-shaped figure in the patterns of the angle of polarization α. Thus, according to Fig. 6B, the radial extension of this eight-figure first decreased, then

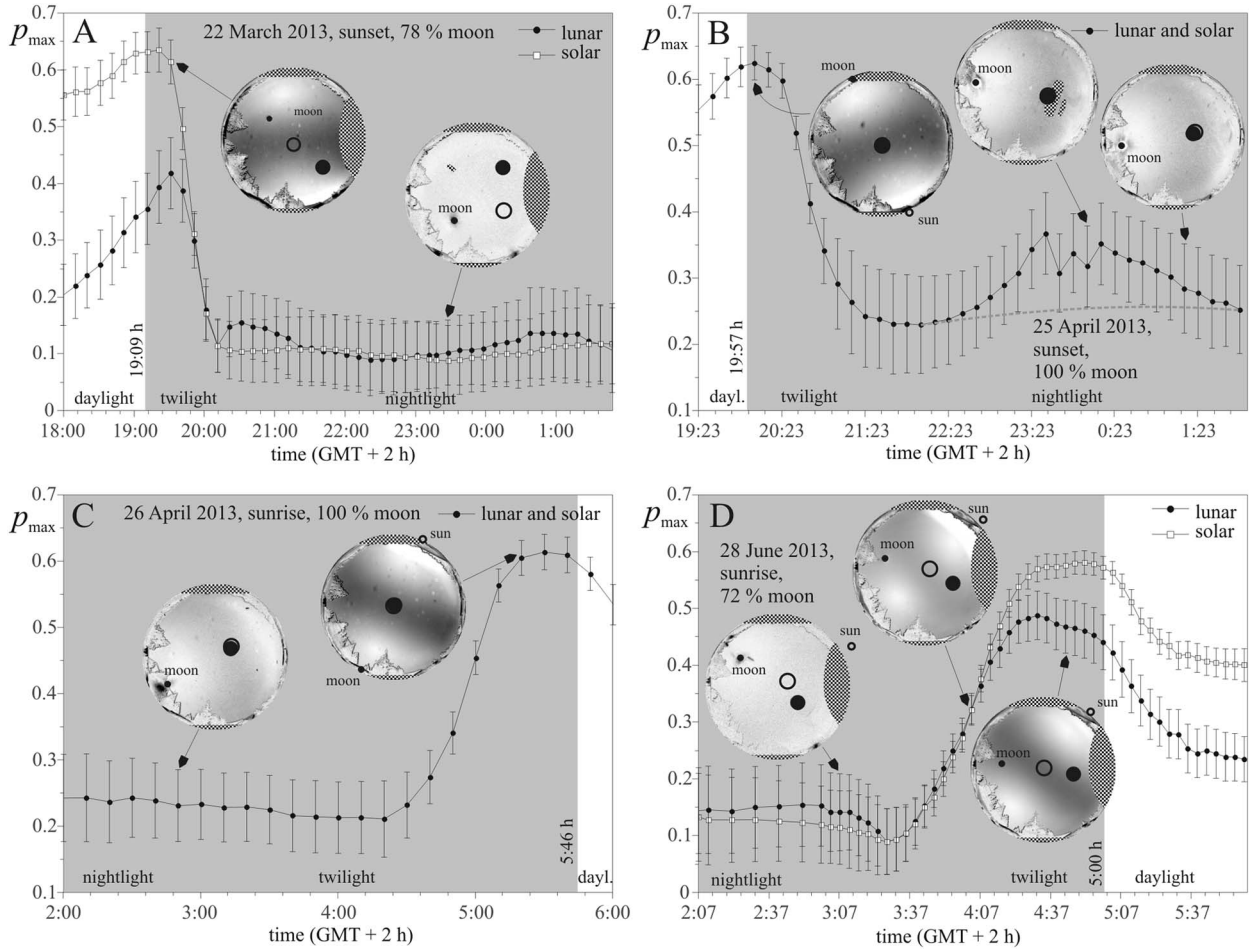

Fig. 5. Maximum p_{max} of the degree of linear polarization p of skylight measured in the green (550 nm) spectral range averaging the p values in small circular celestial regions at 90° from the sun (empty circles) and the moon (solid black circles) as a function of time for the four different situations shown in Figs. 1–4. The vertical bars represent the standard deviation of p_{max}. Insets: typical p patterns belonging to the points of time shown by the arrows. The solar and lunar positions are represented by white and black dots, respectively. The occulted or CCD-void sky regions are marked by a checkered pattern.

increased with time, as can also be seen in Figs. 4C, 4F, and 4I. During twilight and daylight the zenith angle θ_{Ba} of ℓBa increased with wavelength; furthermore θ_{Ba} reached its minimum first in the blue, then in the green, and finally in the red part of the spectrum (Fig. 6B).

Figures 6C and 6D show the same as Figs. 6A and 6B for full moon, when 100% of the moon disc was sunlit (situation as in Figs. (2, 3, 5B, and 5C). According to Fig. 6C, at full moon the symmetry axis of sky polarization was practically the same as the coinciding solar–antisolar and lunar–antilunar meridians. During nighttime and deep twilight the symmetry axis slightly deviated from the mentioned meridians, but this deviation may be the result of noise due to the low intensity of skylight. Near the end of twilight and at daylight this deviation practically disappeared (Fig. 6C). According to Fig. 6D, at full moon the temporal change and dispersion of the zenith angle θ_{Ba} of the lunar Babinet neutral point ℓBa were similar to those observed at partial (72%) moon (Fig. 6B).

Figure 7 demonstrates the dispersion of the direction of the symmetry axis of sky polarization on the pattern of the angle of polarization α prior to sunrise at partial (72%) moon: in the red and green spectral ranges the symmetry axis is near the lunar–antilunar meridian, while in the blue it is already between the lunar–antilunar and solar–antisolar meridians. This situation also occurs in Fig. 6(A).

Figure 8 shows the celestial areas where $p < 10\%$ in the blue spectral range at partial (72%) moon (situation as in Figs. 4 and 5D) at three different points of time. In Fig. 8D the lunar Babinet neutral point ℓBa and the lunar Arago neutral point ℓAr are positioned along the lunar–antilunar meridian, and the symmetry axis of sky polarization coincides with the lunar–antilunar meridian. In Fig. 8E the solar neutral point sN and the lunar neutral point ℓN are along the symmetry axis of celestial polarization. In Fig. 8F the solar Babinet point sBa and the solar Arago point sAr are along the solar–antisolar meridian, and the symmetry axis of sky polarization coincides with the solar–antisolar meridian.

Figures 9B and 9C show the measured (in the blue spectral range) and simulated celestial patterns of the angle of polarization α for partial (72%) moon

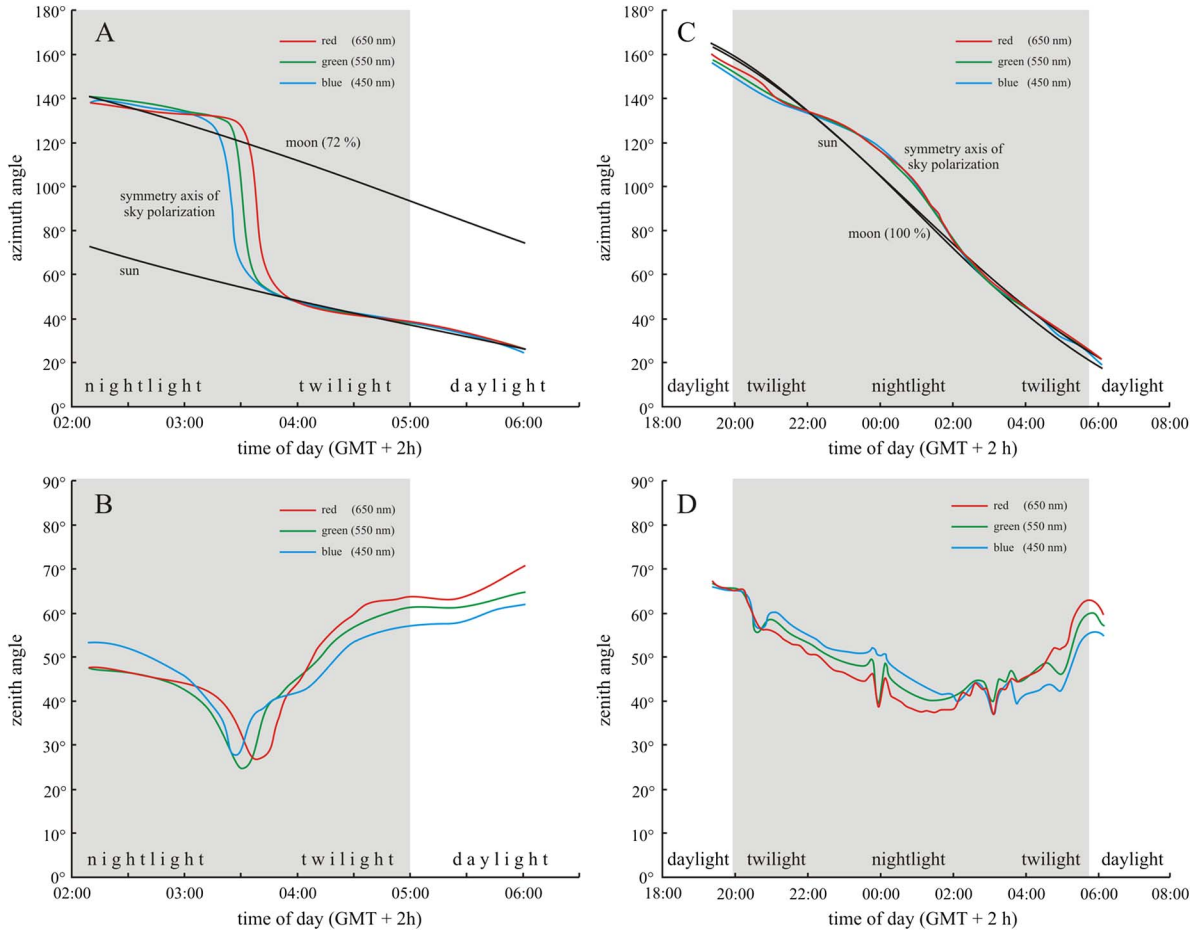

Fig. 6. (A) Azimuth angle of the sun, the moon, and the symmetry axis of the celestial $|\alpha - 90°|$ pattern, where α is the angle of polarization of skylight as a function of time (GMT + 2 h = local summer time) measured by full-sky imaging polarimetry in the red (650 nm), green (550 nm), and blue (450 nm) parts of the spectrum in Szombathely, Hungary (47° 15.481′ N, 16° 36.213′ E) on 28 June 2013 when 72% of the moon disc was sunlit (situation as in Figs. 4 and 5D). (B) Zenith angle of the lunar Babinet neutral point ℓBa (or solar Arago neutral point sAr) versus time for the same case as (A), (C), (D). Same as (A) and (B) on 25–26 April 2013 at full moon when 100% of the moon disc was sunlit (situations as in Figs. 2, 3, 5B, and 5C).

(situation as in Figs. 4 and 5D). The simulation happened for weight $w = 1$, meaning that the contributions of scattered moonlight and skylight to the net polarization of skylight were equal. Although the measured α pattern is noisy, it is qualitatively similar to the simulated α pattern. Figure 9D represents the situation in which the symmetry axis of sky polarization is aligned between the solar–antisolar and lunar–antilunar meridians. In Fig. 9E the neutral points sN and ℓN are positioned within the celestial areas with $p < 10\%$ along the symmetry axis of sky polarization. The neutral points closer to the sun and closer to the moon are called here the solar neutral point (sN) and the lunar neutral point (ℓN), respectively.

All the above results and phenomena can be well seen in the video clips presented (Media1–9).

4. Discussion

Observed from the Earth ground, the clear sky with only one dominating celestial light source (either sun or moon) possesses simultaneously two neutral points [2,3,9,30]: at lower solar elevations (< about 25°–30°) the Babinet point (~25°–30° above the sun) and Arago point (~25°–30° above the antisun), and at higher solar elevations (> about 25°–30°) the Babinet point (~20°–25° above the sun) and the Brewster point (~20°–25° below the sun). From higher (> about 800 m) altitudes from the ground in the atmosphere the fourth neutral point can also be observed ~20°–30° below the antisun [29]. At night similar neutral points (lunar Arago, Babinet, and Brewster) can be observed from the ground, if the moon is visible [28]. These neutral points are always positioned along the solar–antisolar/lunar–antilunar meridian, and their angular distance from the sun/moon and antisun/antimoon depends on the solar/lunar elevation, atmospheric aerosol concentration, and ground reflection [2,3,8,11].

The neutral points sN and ℓN of the twilight sky at partial moon (Figs. 1, 4, 8E, 9C, and 9E) are positioned off the solar–antisolar and lunar–antilunar meridians, and occur only when scattered moonlight and sunlight competes in the moonlit and sunlit

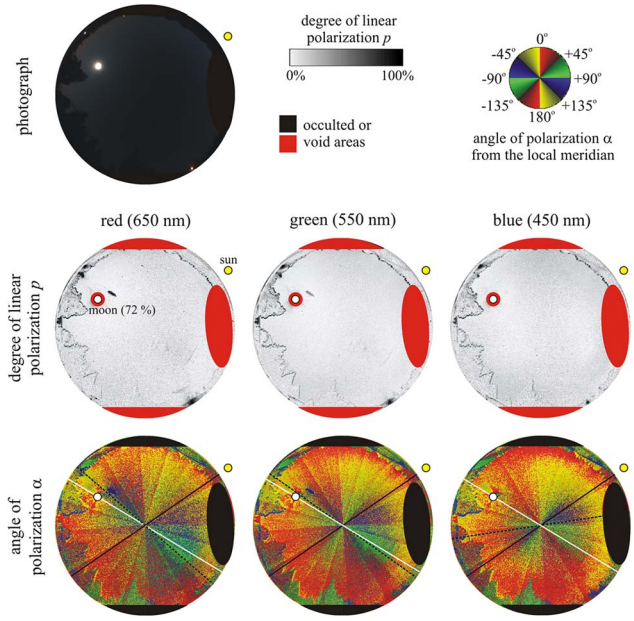

Fig. 7. Photograph and patterns of the degree of linear polarization p and angle of polarization α (clockwise from the local meridian) of the clear sky measured by full-sky imaging polarimetry in the red (650 nm), green (550 nm), and blue (450 nm) parts of the spectrum prior to sunrise in Szombathely, Hungary (47° 15.481′ N, 16° 36.213′ E) at 03:25 (GMT + 2 h) on 28 June 2013 when 72% of the moon disc was sunlit. The positions of the sun (below the horizon) and moon (above the horizon) are shown by yellow and white dots, respectively. In the α patterns black and white continuous lines show the solar–antisolar and lunar–antilunar meridians, respectively, while black dashed lines show the symmetry axis of the $|\alpha - 90°|$ patterns.

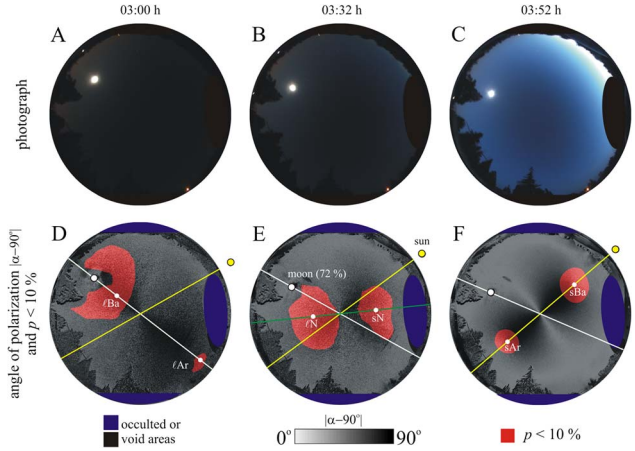

Fig. 8. Measurements performed prior to sunrise on 28 June 2013 in Szombathely, Hungary (47° 15.481′ N, 16° 36.213′ E) when 72% of the moon disc was sunlit (situation as in Figs. 4 and 5D). (A)–(C) Photographs taken at 03:00, 03:32, and 03:52 h (GMT + 2 h), respectively. (D)–(F) Celestial patterns of $|\alpha - 90°|$ in the blue (450 nm) part of the spectrum. Red overlays show the areas of sky where the degree of linear polarization p in the blue (450 nm) is less than 10%. Yellow and white lines show the solar–antisolar and lunar–antilunar meridians, respectively. The positions of the sun (below the horizon) and moon (above the horizon) are shown by yellow and white dots, respectively. ℓBa, lunar Babinet neutral point; ℓAr, lunar Arago neutral point; sN, solar neutral point; ℓN, lunar neutral point; sBa, solar Babinet point; sAr, solar Arago point; green line, symmetry axis of the $|\alpha - 90°|$ pattern.

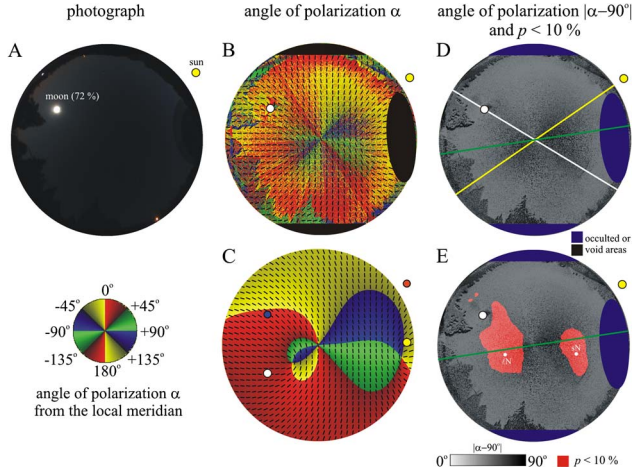

Fig. 9. (A) Photograph of the sky taken on 28 June 2013 at 03:25 (GMT+2 h) in Szombathely, Hungary (47° 15.481′ N, 16° 36.213′ E) when 72% of the moon disc was sunlit (situation as in Figs. 4 and 5D). (B) Pattern of the angle of polarization α of skylight measured in the blue (450 nm) spectral range. Black bars show the average local direction of polarization. (C) Simulated α pattern for the same solar and lunar intensities (with weight $w = 1$, meaning that the contributions of scattered moonlight and skylight to the net polarization of skylight are equal). (D) Celestial pattern of $|\alpha - 90°|$ in the blue (450 nm) part of the spectrum. Yellow and white lines show the solar–antisolar and lunar–antilunar meridians, respectively, while green line represents the symmetry axis of the $|\alpha - 90°|$ pattern. (E) Same as (D) with red overlay showing the areas of sky where the degree of linear polarization p in the blue (450 nm) is less than 10%. sN, solar neutral point; ℓN, lunar neutral point. The positions of the sun (below the horizon) and moon (above the horizon) are shown by yellow and white dots, respectively. Simulated α pattern, where black bars show the average local direction of polarization (Media 8). Simulated α pattern, where white dots show the positions of neutral points. Black line shows the axis of mirror symmetry of sky polarization (Media 9). Both video clips show the patterns from 02:07 to 06:00 h on 28 June 2013 during dawn with weight $w = 1$, meaning that the contributions of scattered sunlight and moonlight to sky polarization are equal. (Yellow and blue dots show the solar and lunar positions, respectively.)

atmosphere prior to sunrise or immediately after sunset. The occurrence of the off-meridian neutral points sN and ℓN of the twilight sky with partial moon is the result of the complex multiple-scattering events in the atmosphere when the intensities of scattered sunlight and moonlight are comparable.

Our finding that p_{max} of light from the twilight sky decreases during the intermediate period (Fig. 5) can also be explained by the multiple scattering of sunlight and moonlight in the atmosphere: when moonlight and sunlight compete, there are two different light sources, the moon and the sun, which both contribute to the atmospheric scattered light field. This enhances the influence of multiple scattering on sky polarization. It is well known that multiple scattering reduces the degree of skylight polarization [3]. The direction of polarization of multiple-scattered light is not always perpendicular to the plane of scattering determined by the dominating celestial light source (sun or moon), the observer,

and the celestial point observed. Light with polarization direction parallel to the scattering plane is called negatively (or abnormally) polarized, while light with polarization perpendicular to the scattering plane is named positively (or normally) polarized [2,3]. Multiple scattering introduces negatively polarized light into the predominantly positively polarized atmosphere. The normal (Arago, Babinet, Brewster, and fourth) neutral points are placed where the intensities of positively and negatively polarized light are equal, and the angle of polarization jumps 90° when crossing a neutral point along its meridian. Hence, the occurrence of neutral points is one of the major consequences of multiple scattering. At twilight, when there are two approximately equally intense celestial light sources, the sun and the moon, the polarization patterns belonging to these two sources interact and form the intermediate two off-meridian neutral points sN and ℓN of the twilight sky at partial moon (Figs. 9C and 9E).

The off-meridian neutral points sN and ℓN of the twilight sky at partial moon have not been observed earlier by researchers of the polarization of twilight skies [27,44,45]. One of the reasons for this is that full-sky imaging polarimetry seems to be necessary for such an observation. Furthermore, these two off-meridian neutral points occur only in a limited (10–20 min) temporal window at partial-moon twilight (Fig. 6A) at low or medium latitudes. Thus, the chance of observing them is tiny relative to that of the normal neutral points observable during the day or night sky for many (8–10) hours.

At full (100%) moon the two neutral points always occur along the solar–antisolar and lunar–antilunar meridians during the polarization transition of the twilight sky. The reason for this is that at full moon the sun and moon are positioned along the coinciding solar/lunar–antisolar/antilunar meridians, and thus the lunar Arago point coincides with the solar Babinet point and the lunar Babinet point coincides with the solar Arago point.

The above-mentioned polarization characteristics of moonlit twilight skies may influence the orientation of the following polarization-sensitive crepuscular/nocturnal animals and the hypothesized sky-polarimetric navigation of sunstone-aided Viking seafarers:

- Dung beetles roll their balls of dung along straight paths after the end of their foraging journey. During ball rolling diurnal dung beetles rely on the sun, and if it is occluded by clouds, on the polarization pattern of the sunlit sky [49]. After sunset and if the moon is not visible, crepuscular and nocturnal ball-rolling dung beetles orient exclusively on the basis of the polarization pattern of the twilight sky. When the moon has risen, the beetles continue to orient along straight paths well after sunset, guided by the sky-polarization pattern created around the moon. The intensity of this dim polarization pattern gradually declines as the moon vanes. Even the extremely dim celestial polarization pattern formed around a crescent moon is sufficient to guide the nocturnal ball-rolling dung beetles along a straight path. A straight-line orientation on these dark nights is performed with the same accuracy and speed as in the case in which dung beetles orient themselves under the much brighter polarization pattern of the sky lit by the sun or the full moon [49].
- The crepuscular and nocturnal tropical halictid bee, *Megalopta genalis*, emerges from its nest in the Panamanian forest beginning approximately 60–45 min before sunrise and forages for 15–30 min before returning accurately to its nest [50]. This behavioral pattern is reversed at sunset. The eyes of this bee species have specializations for extreme dim-light vision [50,51] and appear to be capable of analyzing sky polarization. It is hypothesized that this bee makes use of the celestial polarization pattern during its crepuscular/nocturnal foraging flights.
- An ant species, the night-active Australian bull ant, *Myrmecia pyriformis*, also uses polarized skylight alongside landmark panoramas as a twilight compass cue [52].
- Crepuscularly and/or nocturnally migrating birds also require celestial polarization cues at twilight to set their internal (e.g., geomagnetic) compasses for their flights in the dark, and become disoriented in experiments when provided with a depolarized celestial pattern at this time [32].
- During their orientation/navigation, certain crepuscular/nocturnal aquatic animals (e.g., fish and crustaceans, reviewed in [8]) can also use the polarization pattern of skylight perceived through the Snell's window of the flat water surface [53,54].
- It is a widely discussed and frequently cited hypothesis that Viking navigators might have been able to locate the position of the sun occluded by clouds or below the horizon with a mysterious birefringent crystal, the sunstone (e.g., calcite, tourmaline, or cordierite), on the basis of the pattern of skylight polarization [55–60]. Due to the lack of a magnetic compass, knowledge of the sun position was necessary for their open-sea navigation based on a special sundial [61].

The above-mentioned types of orientation/navigation are based on knowledge of the solar–antisolar or lunar–antilunar meridians coinciding with the mirror symmetry axis of the polarization pattern of the sunlit or moonlit sky, respectively. However, as we showed in this work, at a medium latitude (47° 15.481′ N) during partial-moon twilight there is a short (10–20 min) intermediate period when (i) $p_{\max}$ of skylight polarization decreases, (ii) the two neutral points are off the solar–antisolar and lunar–antilunar meridians, and (iii) from the celestial pattern of the angle of polarization α neither the solar–antisolar nor the lunar–antilunar meridian can be unambiguously determined, which are normally guessed on the basis of the axis of mirror symmetry of the celestial α pattern. Consequently, the above-mentioned animal

orientation and Viking navigation might be impossible during this transient period of partial-moon twilight, the duration of which is considerably enhanced at higher latitudes when the celestial trajectory of the sun and moon runs for a long time near the horizon.

Although this interim period is relatively short (10–20 min) at low and medium latitudes, the consequences of a short-term disorientation due to anomalous celestial polarization must not be underestimated. This is demonstrated well by the example of foraging/flower-visiting honeybees (*Apis mellifera*) that failed to return to their hive after a 2 min period of a total solar eclipse [40–42]. Not only the celestial distribution of intensity and color, but also the patterns of degree p and angle α of skylight polarization, change drastically during the totality of solar eclipses due to the considerably altered illumination conditions [23–25]. The degree of polarization p of light from the eclipsed sky is usually considerably reduced, and if it becomes lower than the threshold p^* of polarization sensitivity of a given species navigating on the basis of sky polarization, the animal can disorient itself. Furthermore, even if $p > p^*$ during totality, the α pattern of the eclipsed sky differs so greatly from that of the normal sky [23–25] that polarization-sensitive animals inevitably disorient themselves when they try to navigate by means of this altered celestial α pattern. Bernáth *et al.* [41] suggested that one of the reasons for the odd disorientated behavior of *Apis mellifera* and their mass perishment (10%–15% of a hive) observed during a total solar eclipse [40,42] may be the unnatural polarization pattern of the eclipsed sky: prior to their flower-visiting flight, honeybee workers fuel up their stomach with an appropriate amount of honey, being proportional to the distance to be traveled from the hive to the nectar source and back to the hive. This distance information is obtained from the messenger bee during her waggle dance in the hive [62]. If a worker bee is disoriented (due to the anomalous celestial polarization pattern during the totality of a solar eclipse, for instance), her fuel can run out before she could find her way back to the hive. In this case the strayed bee perishes inevitably, because she cannot crawl/fly back to the hive.

Another example for animal disorientation elicited by anomalous sky polarization has been reported by Johnson *et al.* [43]: the polarization pattern of the smoky sky during forest fires is more or less anomalous relative to that of the normal sky [17]. In particular, p of skylight is drastically reduced because of the depolarization due to multiple scattering of sunlight on smoke particles. If p of light from a smoky sky is dropped below the threshold p^* of polarization sensitivity of animals using sky polarization for orientation, they can become disoriented. Hegedüs *et al.* [17] suggested that the disorientation of certain insects observed by Johnson *et al.* [43] under smoky skies during the forest fire season in August 2003 in British Columbia was the consequence of the unnaturally weak sky polarization caused by forest fire smoke.

According to Cronin *et al.* [27], animals that use polarized skylight for orientation during the day must solve a difficult geometric problem: while the daytime pattern of sky polarization is fully predictable and strong, it shows complex changes throughout the day as the sun moves across the sky. Similar problems face animals that use nocturnal celestial polarization patterns generated by moonlight. In contrast, during the period from near the onset of astronomical twilight to dawn (or the reverse at dusk), sky polarization has a very constant pattern, varying little in angular distribution, degree of polarization, and spectral content throughout much of this time. In the opinion of Cronin *et al.* [27], if an animal is capable of detecting skylight polarization at very low intensities, the twilight interval could provide a relatively simple orientation cue in the sky. However, our results presented here show that this is not true during the transient period of partial-moon twilight with an anomalous pattern of sky polarization, which makes it impossible to determine the solar–antisolar and lunar–antilunar meridians as the reference direction for orientation/navigation.

The greatest problem that polarization-sensitive animals face when polarization information gradually shifts during twilight at partial moon is to resolve how to reach a destination when the compass being used points in a gradually changing direction. The transient period of this ambiguity could well cause an animal to lose orientation, and the shift to a new polarization compass would seemingly produce a total misorientation into the wrong direction.

This work was supported by the grant OTKA K-105054 (Full-Sky Imaging Polarimetry to Detect Clouds and to Study the Meteorological Conditions Favorable for Polarimetric Viking Navigation) received from the Hungarian Science Foundation by G. Horváth, who also thanks the German Alexander von Humboldt Foundation for an equipment donation and a three-month research fellowship (3.3-UNG/1073032 STP from 1 June to 31 August 2013) in the University of Regensburg. Gyula Szabó thanks for the following grants: OTKA K-104607, Bolyai Research Fellowship of the Hungarian Academy of Sciences, and City of Szombathely under agreement no. S-11-1027. We are grateful to an anonymous reviewer for her/his constructive comments.

References

1. M. L. Brines and J. L. Gould, "Skylight polarization patterns and animal orientation," J. Exp. Biol. **96**, 69–91 (1982).
2. G. P. Können, *Polarized Light in Nature* (Cambridge University, 1985).
3. K. L. Coulson, *Polarization and Intensity of Light in the Atmosphere* (Deepak, 1988).
4. Y. Liu and K. J. Voss, "Polarized radiance distribution measurements of skylight. II. Experiment and data," Appl. Opt. **36**, 8753–8764 (1997).
5. J. A. North and M. J. Duggin, "Stokes vector imaging of the polarized sky-dome," Appl. Opt. **36**, 723–730 (1997).

6. K. J. Voss and Y. Liu, "Polarized radiance distribution measurements of skylight. I. System description and characterization," Appl. Opt. **36**, 6083–6094 (1997).
7. G. Horváth, A. Barta, J. Gál, B. Suhai, and O. Haiman, "Ground-based full-sky imaging polarimetry of rapidly changing skies and its use for polarimetric cloud detection," Appl. Opt. **41**, 543–559 (2002).
8. G. Horváth and D. Varjú, *Polarized Light in Animal Vision Polarization Patterns in Nature* (Springer-Verlag, 2004).
9. G. Horváth and R. Wehner, "Skylight polarization as perceived by desert ants and measured by video polarimetry," J. Comp. Physiol. A **184**, 1–7 (1999).
10. G. Horváth and R. Wehner, "Skylight polarization as perceived by desert ants and measured by video polarimetry," Erratum: J. Comp. Physiol. A **184**, 347–349 (1999).
11. J. Gál, G. Horváth, V. B. Meyer-Rochow, and R. Wehner, "Polarization patterns of the summer sky and its neutral points measured by full-sky imaging polarimetry in Finnish Lapland north of the Arctic Circle," Proc. R. Soc. A **457**, 1385–1399 (2001).
12. I. Pomozi, G. Horváth, and R. Wehner, "How the clear-sky angle of polarization pattern continues underneath clouds: full-sky measurements and implications for animal orientation," J. Exp. Biol. **204**, 2933–2942 (2001).
13. B. Suhai and G. Horváth, "How well does the Rayleigh model describe the E-vector distribution of skylight in clear and cloudy conditions? A full-sky polarimetric study," J. Opt. Soc. Am. A **21**, 1669–1676 (2004).
14. R. Hegedüs, S. Åkesson, and G. Horváth, "Polarization patterns of thick clouds: overcast skies have distribution of the angle of polarization similar to that of clear skies," J. Opt. Soc. Am. A **24**, 2347–2356 (2007).
15. R. Hegedüs, S. Åkesson, R. Wehner, and G. Horváth, "Could Vikings have navigated under foggy and cloudy conditions by skylight polarization? On the atmospheric optical prerequisites of polarimetric Viking navigation under foggy and cloudy skies," Proc. R. Soc. A **463**, 1081–1095 (2007).
16. G. Horváth, R. Hegedüs, A. Barta, A. Farkas, and S. Åkesson, "Imaging polarimetry of the fogbow: polarization characteristics of white rainbows measured in the high Arctic," Appl. Opt. **50**, F64–F71 (2011).
17. R. Hegedüs, S. Åkesson, and G. Horváth, "Anomalous celestial polarization caused by forest fire smoke: why do some insects become visually disoriented under smoky skies?" Appl. Opt. **46**, 2717–2726 (2007).
18. R. Hegedüs, A. Barta, B. Bernáth, V. B. Meyer-Rochow, and G. Horváth, "Imaging polarimetry of forest canopies: how the azimuth direction of the sun, occluded by vegetation, can be assessed from the polarization pattern of the sunlit foliage," Appl. Opt. **46**, 6019–6032 (2007).
19. B. S. Dandekar and J. P. Turtle, "Day sky brightness and polarization during the total solar eclipse of 7 March 1970," Appl. Opt. **10**, 1220–1224 (1971).
20. C. R. N. Rao, T. Takashima, and J. G. Moore, "Polarimetry of the daytime sky during solar eclipses," J. Atmos. Terr. Phys. **34**, 573–576 (1972).
21. G. E. Shaw, "Sky brightness and polarization during the 1973 African eclipse," Appl. Opt. **14**, 388–394 (1975).
22. G. P. Können, "Skylight polarization during a total solar eclipse: a quantitative model," J. Opt. Soc. Am. A **4**, 601–608 (1987).
23. I. Pomozi, J. Gál, G. Horváth, and R. Wehner, "Fine structure of the celestial polarization pattern and its temporal change during the total solar eclipse of 11 August 1999," Remote Sens. Environ. **76**, 181–201 (2001).
24. G. Horváth, I. Pomozi, and J. Gál, "Neutral points of skylight polarization observed during the total eclipse on 11 August 1999," Appl. Opt. **42**, 465–475 (2003).
25. B. Sipőcz, R. Hegedüs, G. Kriska, and G. Horváth, "Spatiotemporal change of sky polarization during the total solar eclipse on 29 March 2006 in Turkey: polarization patterns of the eclipsed sky observed by full-sky imaging polarimetry," Appl. Opt. **47**, H1–H10 (2008).
26. R. Hegedüs, S. Åkesson, and G. Horváth, "Polarization of "water-skies" above arctic open waters: how polynyas in the ice-cover can be visually detected from a distance," J. Opt. Soc. Am. A **24**, 132–138 (2007).
27. T. W. Cronin, E. J. Warrant, and B. Greiner, "Celestial polarization patterns during twilight," Appl. Opt. **45**, 5582–5589 (2006).
28. J. Gál, G. Horváth, A. Barta, and R. Wehner, "Polarization of the moonlit clear night sky measured by full-sky imaging polarimetry at full moon: comparison of the polarization of moonlit and sunlit skies," J. Geophys. Res. D **106**, 22647–22653 (2001).
29. G. Horváth, B. Bernáth, B. Suhai, A. Barta, and R. Wehner, "First observation of the fourth neutral polarization point in the atmosphere," J. Opt. Soc. Am. A **19**, 2085–2099 (2002).
30. G. Horváth, J. Gál, I. Pomozi, and R. Wehner, "Polarization portrait of the Arago point: video-polarimetric imaging of the neutral points of skylight polarization," Naturwissenschaften **85**, 333–339 (1998).
31. M. V. Berry, M. R. Dennis, and R. L. Lee, Jr., "Polarization singularities in the clear sky," New J. Phys. **6**, 162 (2004).
32. R. Muheim, "Behavioral and physiological mechanisms of polarized light sensitivity in birds," Phil. Trans. R. Soc. B **366**, 763–771 (2011).
33. M. J. Freake, "Evidence for orientation using the e-vector direction of polarised light in the sleepy lizard Tiliqua rugosa," J. Exp. Biol. **202**, 1159–1166 (1999).
34. J. S. Auburn and D. H. Taylor, "Polarized light perception and orientation in larval bullfrogs *Rana catesbeiana*," Anim. Behav. **27**, 658–668 (1979).
35. I. Novales-Flamarique and H. I. Browman, "Foraging and prey-search behavior of small juvenile rainbow trout (*Oncorhynchus mykiss*) under polarized light," J. Exp. Biol. **204**, 2415–2422 (2001).
36. T. Labhart and E. P. Meyer, "Detectors for polarized skylight in insects: a survey of ommatidial specializations in the dorsal rim area of the compound eye," Microsc. Res. Tech. **47**, 368–379 (1999).
37. S. M. Goddard and F. B. Forward, "The role of the underwater polarized light pattern, in sun compass navigation of the grass shrimp, *Palaemonetes vulgaris*," J. Comp. Physiol. A **169**, 479–491 (1991).
38. S. Åkesson and A. Hedenström, "How migrants get there: migratory performance and orientation," BioScience **57**, 123–133 (2007).
39. R. Muheim, J. B. Phillips, and S. Åkesson, "Polarized light cues underlie compass calibration in migratory songbirds," Science **313**, 837–839 (2006).
40. L. Baldavári, "Change of honeybee behavior in an apiary during the total solar eclipse on 11 August 1999," Állattani Közlemények **86**, 137–143 (2001) (in Hungarian).
41. B. Bernáth, I. Pomozi, J. Gál, G. Horváth, and R. Wehner, "Skylight polarization during the total solar eclipse of 11 August 1999 and its possible biological implications," Állattani Közlemények **86**, 81–92 (2001) (in Hungarian).
42. F. Szentkirályi and L. Szalay, "Influence of the total solar eclipse of 11 August 1999 on the behavior and collecting activity of honeybees," Állattani Közlemények **86**, 115–136 (2001) (in Hungarian).
43. D. L. Johnson, D. Naylor, and G. Scudder, "Red sky in day, bugs go astray," in annual *Meeting of the Canadian Association of Geographers, Western Division*, Lethbridge, Alberta, Canada, 12 March 2005, Conference Abstracts, p. 145.
44. J. V. Dave and K. R. Ramanathan, "On the intensity and polarisation of the light from the sky during twilight," Proc. Indian Acad. Sci. A **43**, 67–68 (1955).
45. G. V. Rozenberg, *Twilight: A Study in Atmospheric Optics* (Plenum, 1966).
46. J. Meeus, *Astronomical Algorithms*, 2nd ed. (Willmann-Bell, 1998).
47. M. R. Teague, "Image analysis via the general theory of moments," J. Opt. Soc. Am. **70**, 920–930 (1980).
48. R. M. A. Azzam and N. M. Bashara, *Ellipsometry and Polarized Light* (North-Holland, 1989).

49. M. Dacke, P. Nordström, and C. H. Scholtz, "Twilight orientation to polarized light in the crepuscular dung beetle *Scarabaeus zambesianus*," J. Exp. Biol. **206**, 1535–1543 (2003).
50. E. J. Warrant, A. Kelber, A. Gislen, B. Greiner, W. Ribi, and W. Wcislo, "Nocturnal vision and landmark orientation in a tropical halictid bee," Curr. Biol. **14**, 1309–1318 (2004).
51. B. Greiner, W. A. Ribi, and E. J. Warrant, "Retinal and optical adaptations for nocturnal vision in the halictid bee *Megalopta genalis*," Cell Tissue Res. **316**, 377–390 (2004).
52. S. F. Reid, A. Narendra, J. M. Hemmi, and J. Zeil, "Polarized skylight and the landmark panorama provide night-active bull ants with compass information during route following," J. Exp. Biol. **214**, 363–370 (2011).
53. G. Horváth and D. Varjú, "Underwater refraction-polarization patterns of skylight perceived by aquatic animals through Snell's window of the flat water surface," Vis. Res. **35**, 1651–1666 (1995).
54. S. Sabbah, A. Barta, J. Gál, G. Horváth, and N. Shashar, "Experimental and theoretical study of skylight polarization transmitted through Snell's window of a flat water surface," J. Opt. Soc. Am. A **23**, 1978–1988 (2006).
55. T. Ramskou, "Solstenen," Skalk **2**, 16–17 (1967).
56. C. Roslund and C. Beckman, "Disputing Viking navigation by polarized skylight," Appl. Opt. **33**, 4754–4755 (1994).
57. B. E. Schaefer, "Vikings and polarization sundials," Sky and Telescope **93**, 91–94 (1997).
58. G. Horváth, A. Barta, I. Pomozi, B. Suhai, R. Hegedüs, S. Åkesson, B. Meyer-Rochow, and R. Wehner, "On the trail of Vikings with polarized skylight: experimental study of the atmospheric optical prerequisites allowing polarimetric navigation by Viking seafarers," Phil. Trans. R. Soc. B **366**, 772–782 (2011).
59. B. Bernáth, M. Blahó, Á. Egri, A. Barta, and G. Horváth, "An alternative interpretation of the Viking sundial artefact: an instrument to determine latitude and local noon," Proc. R. Soc. A **469**, 20130021 (2013).
60. B. Bernáth, M. Blahó, Á. Egri, A. Barta, G. Kriska, and G. Horváth, "Orientation with a Viking sun-compass, a shadow-stick, and two calcite sunstones under various weather conditions," Appl. Opt. **52**, 6185–6194 (2013).
61. S. Thirslund, *Viking Navigation: Sun-Compass Guided Norsemen First to America* (Bogtrykkeri a-s, Skjern, 2001).
62. K. von Frisch, *The Dance Language and Orientation of Bees* (Harvard University, 1967).